Molecular Biology of the Cell
Vol. 17, 4069–4079, September 2006

Measuring Nanometer Scale Gradients in Spindle Microtubule Dynamics Using Model Convolution Microscopy[D] [V]

Chad G. Pearson,*† Melissa K. Gardner,†‡ Leocadia V. Paliulis,§ E. D. Salmon,§ David J. Odde,‡ and Kerry Bloom§

*Department of Molecular, Cellular, and Developmental Biology, University of Colorado at Boulder, Boulder, CO 80309-0347; ‡Department of Biomedical Engineering, University of Minnesota, Minneapolis, MN 55455; and §Department of Biology, University of North Carolina at Chapel Hill, Chapel Hill, NC 27599-3280

Submitted April 17, 2006; Revised June 9, 2006; Accepted June 20, 2006
Monitoring Editor: Orna Cohen-Fix

A computational model for the budding yeast mitotic spindle predicts a spatial gradient in tubulin turnover that is produced by kinetochore-attached microtubule (kMT) plus-end polymerization and depolymerization dynamics. However, kMTs in yeast are often much shorter than the resolution limit of the light microscope, making visualization of this gradient difficult. To overcome this limitation, we combined digital imaging of fluorescence redistribution after photobleaching (FRAP) with model convolution methods to compare computer simulations at nanometer scale resolution to microscopic data. We measured a gradient in microtubule dynamics in yeast spindles at ~65-nm spatial intervals. Tubulin turnover is greatest near kinetochores and lowest near the spindle poles. A β-tubulin mutant with decreased plus-end dynamics preserves the spatial gradient in tubulin turnover at a slower time scale, increases average kinetochore microtubule length ~14%, and decreases tension at kinetochores. The β-tubulin mutant cells have an increased frequency of chromosome loss, suggesting that the accuracy of chromosome segregation is linked to robust kMT plus-end dynamics.

INTRODUCTION

Budding yeast is an important genetic model system for studying the mechanisms of accurate mitotic chromosome segregation. In metaphase, chromosomes become aligned with one sister kinetochore attached to the microtubule plus-end from one spindle pole and the other sister attached to the plus-end from the opposite spindle pole before chromosome segregation in anaphase. This amphitelic kinetochore attachment and chromosome biorientation allows sister kinetochores to pull and stretch their intervening centromeric chromatin, thereby generating tension at kinetochores that promotes stability of kMT plus-end attachment (Inoue and Salmon, 1995; Nicklas, 1997). Force generation for stretching centromeres, aligning chromosomes, and segregating sister chromatids is coupled to changes in kMT length (Maddox *et al.*, 2000; Pearson *et al.*, 2001; Gardner *et al.*, 2005). With kMT plus-end depolymerization, kinetochores pull chromosomes poleward. Conversely, kinetochores move away from the poles with kMT plus-end polymerization, thereby reducing kinetochore tension. Kinetochores could also be pulled poleward by flux, which is coupled to depolymerization at pole-anchored kMT minus ends (Kapoor and Compton, 2002; Mitchison, 2005). Poleward flux occurs by the net addition of tubulin subunits at the microtubule plus-end and subtraction of subunits at the minus-end, whereas kinetochores remain attached to spindle-pole anchored kMTs. This generates poleward forces on kinetochores during mitosis. However, in budding yeast, evidence so far indicates that kMT minus-ends are capped (indicating no microtubule minus-end disassembly), that flux does not occur, and that kinetochore movements depend only on kMT plus-end dynamics (Byers *et al.*, 1978; Rout and Kilmartin, 1990; Bullitt *et al.*, 1997; O'Toole *et al.*, 1999; Maddox *et al.*, 2000; Tanaka *et al.*, 2005).

Unlike tissue cells, budding yeast kinetochores gain attachment to a single kMT nucleated from the spindle pole (Peterson and Ris, 1976; Winey *et al.*, 1995; O'Toole *et al.*, 1999). Because microtubules are singly attached to kinetochores, kMT plus-end dynamics can be directly linked to centromere stretching and thus tension generated at the kinetochore (Goshima and Yanagida, 2000; He *et al.*, 2000; Tanaka *et al.*, 2000; Pearson *et al.*, 2001). Dynamic kMTs mediate kinetochore position, and thus kinetochores become clustered to average metaphase positions on either side of the spindle equator. Kinetochore congression to the equatorial metaphase plate requires spatial cues along the spindle length so that kinetochores can detect the spindle equator. One possible model for this is a spatial gradient in the regulation of microtubule dynamics predicted by our earlier modeling studies (Sprague *et al.*, 2003; Gardner *et al.*, 2005).

Previously, we used simulations of kMT microtubule dynamics to study how kMTs could facilitate chromosome congression in yeast (Sprague *et al.*, 2003; Pearson *et al.*, 2004; Gardner *et al.*, 2005). In our model, kinetochore microtubule dynamics are regulated by 1) a spatial gradient between the spindle poles and 2) tension generated from centromere

This article was published online ahead of print in *MBC in Press* (http://www.molbiolcell.org/cgi/doi/10.1091/mbc.E06–04–0312) on June 28, 2006.

[D] [V] The online version of this article contains supplemental material at *MBC Online* (http://www.molbiolcell.org).

† These authors contributed equally to this work.

Address correspondence to: Kerry Bloom (kbloom@email.unc.edu).

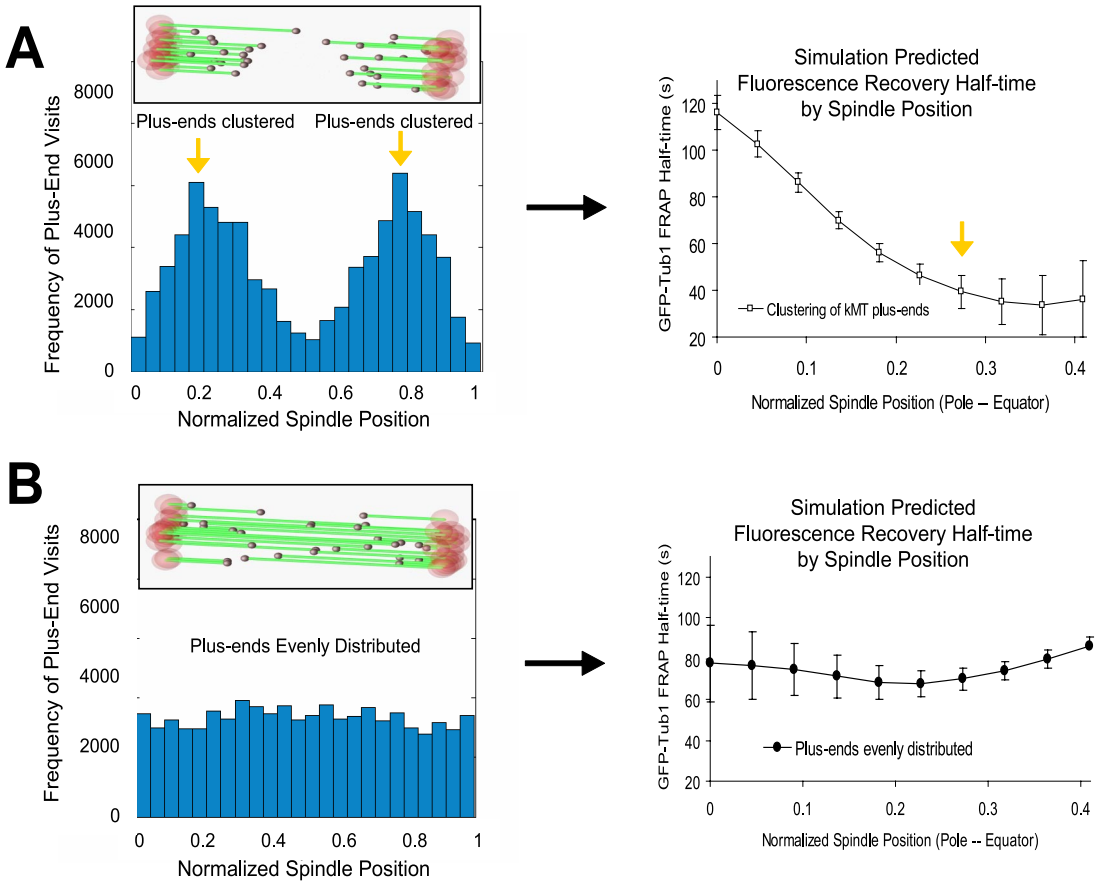

Figure 1. Simulation of yeast metaphase predicts kMT plus-end clustering and a spatial gradient in kMT tubulin turnover. (A) In a model with spatial catastrophe and rescue gradients, kMT plus-ends and kinetochores cluster on either side of the spindle equator, even though kMT growth and shortening rates are constant. In this model, there is an approximately Gaussian distribution of kMT plus-end positions over the half-spindle, with kMT plus-ends frequently midway between the SPB and the spindle equator (left, yellow arrows). The cartoon represents a yeast mitotic spindle with kinetochore clustering on either side of the spindle equator. SPB, red; microtubules, green; kinetochores, gray. A spatial gradient in tubulin turnover rate was predicted from this model. Turnover was most rapid at the location of plus-end clustering (right, yellow arrow; bleached half-spindle only). (B) In a stochastic dynamic instability model where catastrophe and rescue frequencies are constant and equal over the spindle length there is approximately a uniform distribution of kMT plus-ends (left), and no spatial gradient in tubulin turnover was predicted (right). The cartoon represents a theoretical mitotic spindle with no obvious kinetochore clustering and plus-ends are randomly distributed along the spindle length.

stretch. The spatial gradient promotes catastrophe of kMT plus-ends at the center of the spindle and suppresses catastrophe near the spindle poles. This gradient is sufficient to establish basic spindle bipolarity so that kinetochores are usually clustered midway between the pole and the equator. In addition, tension promotes microtubule plus-end rescue and lack of tension suppresses rescue, which acts to correct most of the residual equator crossing events. Together, these mechanisms lead to clustering of sister kinetochores on either side of the spindle equator, with high fidelity of kinetochores to their respective half-spindle (Gardner *et al.*, 2005).

A new prediction of this model is that a spatial gradient in kMT turnover should be established over the length of the spindle, such that tubulin turnover is highest near the kinetochores and lowest near the spindle pole. Clustering of sister kinetochores on either side of the spindle equator is predicted to result in rapid tubulin turnover specifically where kinetochore-attached microtubule plus-ends are clustered on either side of the spindle equator. This is achieved by spatial variation of kMT catastrophe and rescue frequencies over the length of the spindle, even though the rates of kMT polymerization and depolymerization remain constant. Thus, spatial variation in the parameters of kMT dynamic instability, specifically in catastrophe and rescue frequency, predict a spatial gradient in tubulin turnover over the spindle length. Previous GFP-tubulin FRAP studies measured the average half-life of tubulin within kMTs to be ~50 s (Maddox *et al.*, 2000), but no attempt was made to detect a gradient in FRAP half-times because the average length of kinetochore microtubules at metaphase (~390 nm; Winey *et al.*, 1995) was approximately equal to the extent of microscope blur, as quantified by the point-spread function (PSF). Because the length of the proposed tubulin turnover gradient in yeast is close to or even less than the theoretical resolution limit of the light microscope (~220 nm at 510-nm wavelength [GFP] by the Rayleigh criterion), detection of such a gradient presents a technical challenge (Fowles, 1975).

To overcome this potential limitation, we have combined a technically improved GFP-tubulin FRAP assay with model convolution microscopy methods to quantify tubulin turnover in spindle MTs. This improved FRAP technique provided 1) increased temporal resolution and 2) a collection of microtubule turnover data at ~65-nm spatial sampling in-

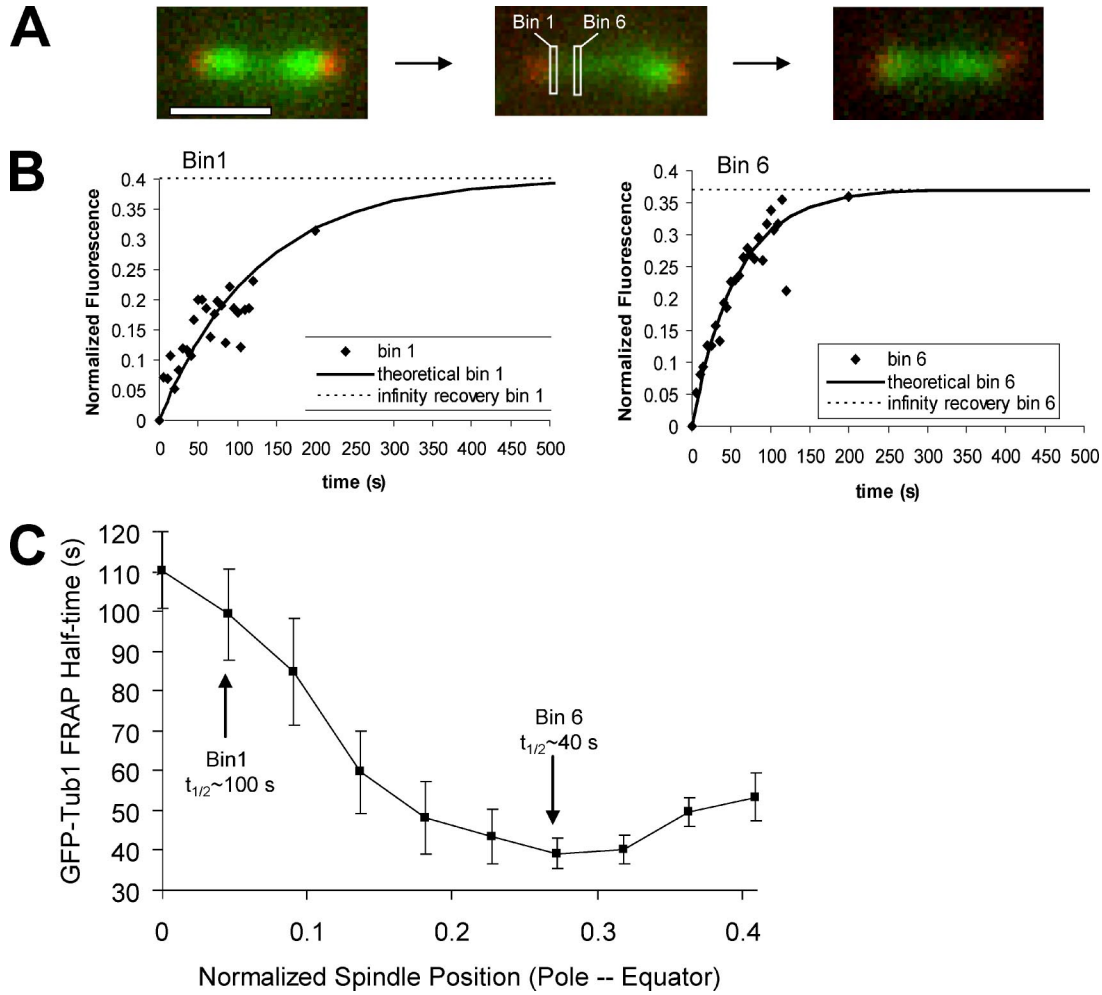

Figure 2. Spindle microtubules exhibit a spatial gradient in tubulin turnover rate. (A) Experimental images of the GFP tubulin FRAP experiment (SPB, red; MTs, green). Experimental fluorescence recovery was monitored in ~65-nm "bins" along the photobleached half of the mitotic spindle (white boxes are unscaled representative bins). Scale bar, 1000 nm. (B) Representative raw experimental data from a bin near the SPB (left, bin1), and a bin midway between the spindle equator and the SPB (right, bin 6). Theoretical exponential fit curves calculated based on bin experimental recovery half-times are drawn through each plot (solid line). (C) Quantitative experimental results for GFP-tubulin FRAP half-time by spindle location. Normalized spindle position 0 represents the bin nearest the SPB, whereas normalized spindle position 0.45 represents the bin near the spindle equator. FRAP was most rapid at spindle positions midway between the spindle equator and each SPB, where plus-ends were clustered in the metaphase spindle (~bin 6).

tervals along the length of the mitotic spindle. The positions of fluorescent microtubules in computer simulations of dynamic kMTs were convolved with the three-dimensional microscope PSF (model convolution microscopy) to reproduce the spatially resolved FRAP experiment. The statistically defined agreement between the experimental microscopic data and the simulated images in turn defined the valid parameter values for the spatial gradient in kMT plus-end dynamics.

A prediction of the model was that reduced kMT plus-end dynamics should preserve the FRAP gradient at a slower time scale and produce a tighter clustering of sister kinetochores on either side of the spindle equator. The optimal positioning of kinetochores and attached kMT plus-ends was defined by the spatial regulation of kMT catastrophe and rescue frequencies (Gardner *et al.*, 2005). The length of plus-end excursions away from this optimal position on either side of the spindle equator depended directly on the growth and shortening velocities of the plus-ends. With rapid growth and shortening velocities, longer kMT growth and shortening excursions away from the most stable (mean) position were possible. This resulted in weak clustering of kMT plus-ends. Alternatively, slower kMT plus-end growth and shortening velocities lead to tighter clustering of kinetochores in the model, as kMT plus-ends are less likely to make longer excursions away from their most stable position. We tested this prediction using a β-tubulin mutant (*tub2C354S*) that suppresses microtubule plus-end dynamics (Gupta *et al.*, 2002). The gradient in tubulin turnover was preserved and kinetochores were more tightly clustered in β-tubulin mutant metaphase spindles. This indicated that the regulation of kMT dynamics required to produce kinetochore clustering on either side of the spindle equator was maintained. Surprisingly, we also discovered that centromere stretch was reduced, and chromosome loss increased in the β-tubulin mutant. The higher chromosome loss rate suggested there is a link between average kinetochore tension, as dictated by microtubule dynamics, and the accuracy of chromosome segregation.

Table 1. Simulation parameters

	Wild-type experimental, cytoplasmic microtubules	Wild-type simulation, kMT dynamics	*tub2-C354S* experimental, cytoplasmic microtubules	*tub2-C354S* simulation, kMT dynamics
Growth rate (Vg; μm/min)	1.30 ± 0.42	1.20 ± 0.10[a]	0.23 ± 0.11	0.40 ± 0.10[d]
Shrinkage rate (Vs; μm/min)	1.98 ± 0.68	1.20 ± 0.10[a]	0.42 ± 0.18	0.40 ± 0.10[d]
Catastrophe frequency (k_c; min^{-1})	0.46 ± 0.10	0.25–27[a]	0.024 ± 0.009	0.25–27[b]
Basal rescue frequency (k_r; min^{-1})	0.21 ± 0.07	9[c]	0.036 ± 0.012	11[c]

[a] Calculated probability of fits (p value): Vg = Vs = 1.2 μm/min, p = 0.42; Vg = Vs = 1.1 μm/min, p = 0.36; Vg = Vs = 1.3 μm/min, p = 0.08. p values calculated as described in Sprague *et al.* (2003). Growth and shortening velocities are assumed to be equal for all simulations.

[b] Model catastrophe frequency depends on spindle position (Supplementary Material and Gardner *et al.*, 2005).

[c] Model rescue frequency depends on the extension between sister kinetochores, as measured by distance between assigned sister kinetochores in the simulation (Supplementary Material and Gardner *et al.*, 2005). Reported value is for lowest basal rescue frequency in the absence of tension.

[d] Calculated probability of fits (p value): Vg = Vs = 0.40 μm/min, p = 0.40; Vg = Vs = 0.30 μm/min, p = 0.14; Vg = Vs = 0.50 μm/min, p = 0.24.

MATERIALS AND METHODS

Yeast Strains and Cell Culture

The strains used in this study were KBY2129 (*MAT***a**, *LEU2::GFP-TUB1::leu2Δ1, SPC29RFPKAN, trp1-63 leu2-1 ura3-52 his3-200 lys2-801*), KBY2012 (*MAT***a**, *SPC29CFPKAN, cse4::HB,* pKK1, *trp1-63 leu2-1 ura3-52 his3-200 lys2-801*), KBY2700GT (*MAT*a, *LEU2::GFP-TUB1::leu2Δ1, SPC29RFPKAN, trp1 Δ 63, his4-917, ura3-52, TUB1, TUB2*), KBY2701GT (*MAT*a, *LEU2::GFP-TUB1::leu2Δ1, SPC29RFPKAN, trp1Δ63, his4-917, URA3/ura3-52, TUB1, tub2-C354S*), KBY2702 (*MAT*a, *SPC29CFPKAN, cse4::HYG,* pKK1, *trp1 Δ 63, his4-917, ura3-52, TUB1, TUB2*), KBY2703 (*MAT*a, *SPC29CFPKAN, cse4::HYG,* pKK1, *SPC29RFPKAN, trp1Δ63, his4-917, URA3/ura3-52, TUB1, tub2-*C354S), KBY2700RS (*MAT*a, *SPC29RFPKAN, leu2Δ1, trp1Δ63, his4-917, URA3/ura3-52, TUB1, tub2-C354S,* pRS315) and KBY2701RS (*MAT*a, *SPC29RFPKAN, leu2Δ1, trp1Δ63, his4-917, URA3/ura3-52, TUB1, tub2-C354S,* pRS315). The strains listed above are adapted from those described by Gupta *et al.* (2002). pKK1 is a pRS314-based plasmid containing the centromere specific histone-H3 variant, *CSE4*, fused to *GFP* (Chen *et al.*, 2000; Pearson *et al.*, 2001).

Cell growth techniques and conditions were performed as previously described (Pearson *et al.*, 2003, 2004; Gardner *et al.*, 2005).

Fluorescence Imaging and Photobleaching

Imaging techniques were performed as previously described (Pearson *et al.*, 2001, 2003, 2004). The general FRAP techniques performed were previously described (Maddox *et al.*, 2000; Pearson *et al.*, 2003). In this study, the microscope used for FRAP was a Nikon Eclipse TE2000E stand (Melville, NY) with 100× PlanApo NA 1.4 objective with a Hamamatsu Orca ER camera (Bridgewater, NJ). The microscope back port was fitted with a Point Source (Southampton, United Kingdom) beam expander fiber optically coupled to a SpectraPhysics (Mountain View, CA) 50-mW argon ion laser to bring the photobleaching light into the back aperture of the objective. The laser exposure was 25 ms with light attenuated by neutral density. Fluorescent images were acquired at intervals between 2 s and 2 min, depending on the experiment.

To ensure the spindle was in focus, we included Spc29RFP labeled SPBs to mark the spatial position of GFP-Tub1 fluorescence redistribution relative to the SPB. For increased temporal resolution, only single image planes were acquired.

Data Analysis

Analysis of FRAP experiments to determine fluorescence redistribution half-times ($t_{1/2}$) was performed as previously reported (Maddox *et al.*, 2000), except that raw fluorescence data were collected for every unbinned camera pixel (~65 nm). To collect accurate fluorescence recovery data by position along the length of the spindle, poles markers were included in the assay and were used to provide a frame of reference for image analysis. Spindles in which one or both pole markers moved out of focus during the experiment were rejected. Fluorescence was collected over the length of the spindle and then integrated over 15 pixels perpendicular to the centerline of the spindle at each spindle position using MATLAB (Version 6.0, MathWorks, Natick, MA) as previously described (Sprague *et al.*, 2003; Gardner *et al.*, 2005). To account for variations in spindle length, integrated data at each spindle position were then averaged into 24 bins per spindle, such that each bin contained data from 1 to 2 pixels (typically 1 pixel), depending on spindle length. Data for each of

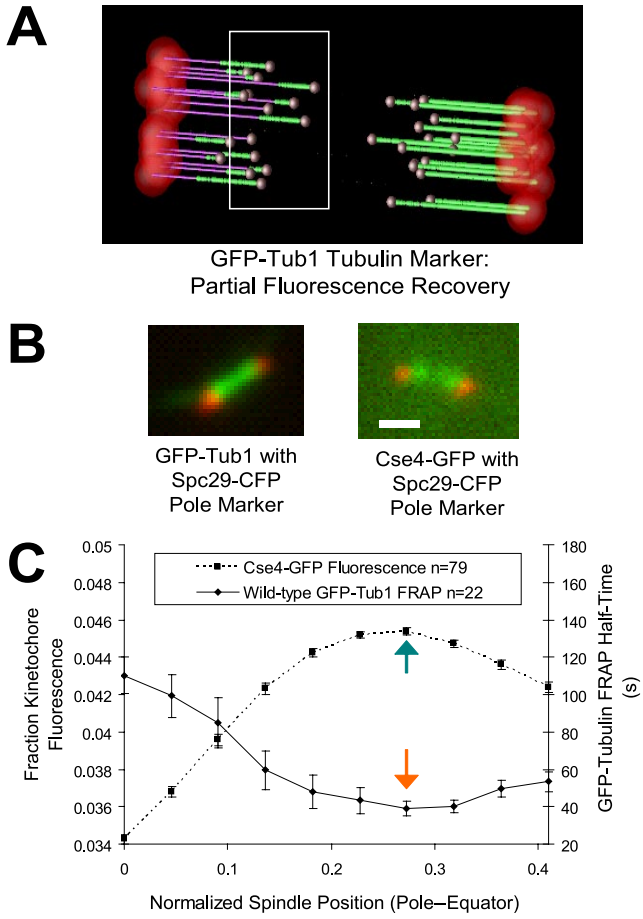

Figure 3. Kinetochores are clustered at positions of most rapid GFP-tubulin exchange. (A) The animated simulation output revealed a link between GFP-tubulin FRAP and kinetochore positioning, such that turnover is predicted to be most rapid in locations of kinetochore clustering (white box, Supplementary Movie 1). SPB, red; unbleached kMTs, green; kinetochores, gray; and photobleached kMTs, violet). (B) Representative experimental spindle images of Tub1-GFP with Spc29-RFP spindle pole markers (left) and Cse4-GFP with Spc29-CFP spindle pole markers (right). (C) Comparison of kinetochore position (Cse4-GFP) with GFP-tubulin FRAP. The peak in kinetochore localization corresponds to the site of most rapid GFP-tubulin FRAP.

Table 2. Spindle statistics

Spindle description	GFP-Tub1 FRAP half-time ($t_{1/2}$; s)[a]	Spindle length (nm)	XSPB to kinetochore distance (nm)[b]	Kinetochore cluster spacing (nm)[c]	Corrected mean kMT length (nm)	n
Wild-type spindles	65 ± 31 (n = 22)	1610 ± 200	430 ± 130	750 ± 280	380 ± 130	79
tub2C354 spindles	146 ± 64 (n = 10)	1530 ± 230	490 ± 90	560 ± 230	440 ± 90	121

Values are mean ± SD.

[a] The mean was calculated over a 10-pixel span from the SPB toward the equator.

[b] Estimated by multiplying the normalized spindle location of peak mean kinetochore-associated fluorescence by the mean spindle length.

[c] Calculated as follows: (mean spindle length) − (2∗SPB to kinetochore distance).

the 24 bins along the length of the spindle were averaged over all of the experiments. Fluorescence recovery half-times ($t_{1/2}$) were calculated based on the recovery profile of each bin as previously described (Maddox *et al.*, 2000).

Kinetochore localization, as measured by Cse4-GFP fluorescence, was measured as described previously (Sprague *et al.*, 2003; Gardner *et al.*, 2005).

Simulation Methods

Simulation of the GFP-tubulin FRAP experiment was performed as previously described (Gardner *et al.*, 2005), with the exception that fluorescence was calculated for every pixel during recovery to provide a comparison with experimental results. kMT dynamics were simulated via MATLAB, with simulated images generated at specified time points to correspond to experimental values. The bleach status of every incorporated and free-pool GFP-tubulin dimer was recorded at every time point in the simulation. FRAP was then realized as unbleached GFP-tubulin dimers were incorporated into bleached MTs via plus-end polymerization. Simulated fluorescence values by pixel were then normalized into 24 bins, as described above.

In the current simulation, interpolar microtubules (ipMTs; of which we assumed there were eight, vs. 32 kMTs) were considered to be nondynamic (Maddox *et al.*, 2000) and to run the length of the spindle (Peterson and Ris, 1976; Winey *et al.*, 1995). We tested the effect of dynamic ipMTs on the GFP-tubulin FRAP simulation, and assuming similar growth and shortening rates between kMTs and ipMTs, dynamic ipMTs had little effect on FRAP half-times where kMT fibers were relatively abundant (Supplementary Figure S1).

Plasmid Loss Assays

For plasmid loss experiments, KBY2700RS and KBY2701RS were grown in SD-Leu media to midlogarithmic growth before dilution into SD-complete (nonselective) media and grown for 17 h at 24°C. Cells were then plated onto SD-complete plates before replica plating to SD-complete and SD-Leu. Three separate experiments were performed. The plasmid loss percentage was then calculated by determining the ratio of colonies found on the selective versus nonselective media.

RESULTS

Simulations Predict Rapid Tubulin Turnover at Sites of kMT Plus-end Clustering

To understand how the regulation of microtubule dynamics could facilitate kinetochore clustering and metaphase alignment, GFP-tubulin FRAP experiments were simulated for yeast metaphase spindles (*Materials and Methods*). In the simulation, kMT growth and shortening was assumed to take place at the kMT plus-ends, and the polymerization and depolymerization rates of kMT plus-ends were assumed to be constant over the spindle length. This assumption is made for simplicity in parameter evaluation and is supported by previous measurements of cytoplasmic microtubule dynamics, in which growth and shortening rates were similar (see Table 1; Gupta *et al.*, 2002). However, the simulated catastrophe and rescue frequency were not constant over the length of the spindle. A spatial gradient in catastrophe and rescue frequency results in kinetochore (and thus kMT plus-end) clustering on either side of the spindle equator as is experimentally observed during yeast metaphase. The GFP-tubulin FRAP simulation predicted that clustering of kMT plus-ends in the mitotic spindle results in a spatial variation of tubulin turnover rate over the length of the spindle, such that turnover will be most rapid in the location of plus-end clustering, with a decreased rate of turnover elsewhere (Figure 1A; Supplementary Movie 1). Alternatively, simulations with constant catastrophe and rescue frequency over the length of the spindle do not predict kinetochore and kMT plus-end clustering on either side of the spindle equator (Figure 1B). In simulations where catastrophe and rescue frequency are constant, the distribution of kMT plus-ends was even over the length of the spindle, and thus no gradient in tubulin turnover was predicted (Figure 1B; Supplementary Movie 2).

GFP-Tubulin Turnover Varies as a Function of Position within the Mitotic Spindle

To test whether kMT turnover rates vary as a function of spindle position, as predicted by the spatial catastrophe and rescue frequency gradients in the model (Figure 1A), we used laser photobleaching to selectively bleach one-half of a yeast metaphase spindle labeled with GFP-tubulin. Photobleaching was performed using a diffraction-limited spot from the 488-nm line of an Argon-ion laser, and recovery was followed by high-resolution digital imaging, initially acquiring images at ~2-s intervals and then increasing the time interval. Fluorescence was collected at each pixel cross-section for the CCD camera along the length of the spindle and then integrated over 15 pixels perpendicular to the centerline of the spindle at each spindle position or "bin" (Figure 2, A and B; *Materials and Methods*). This allowed for monitoring of fluorescence recovery separately in each camera pixel (~65-nm width) along the length of the yeast metaphase spindle. We found that GFP-tubulin FRAP was indeed fastest where plus-ends were clustered, midway between the spindle equator and each SPB (Figure 2C).

The time to half-maximal recovery was then calculated for the entire bleached half-spindle at subdiffraction limited sampling (~65 nm) intervals along the length of the spindle (Figure 2C). The mean half-time ($t_{1/2}$) for GFP-tubulin FRAP was ~110 s near the SPB and ~40 s midway between the SPB and the spindle equator. The average $t_{1/2}$ of 65 ± 31 s is in agreement with previously reported values of 52 ± 23 s for wild-type spindles (Maddox *et al.*, 2000; $p = 0.33$). In some cases, adjacent sampling intervals were statistically different ($p < 0.05$, by *t* test, Supplementary Table S1). A slight upturn in GFP-tubulin half-times was observed near the equator, as predicted by the model (Figure 1A). The experimentally observed upturn was slightly larger, but not significantly different from that predicted by the model.

The experimental results are quantitatively consistent with the plus-end clustering model predictions ($p = 0.42$, parameter values Table 1; Figure 1A), and inconsistent with a model that does not exhibit plus-end clustering, regardless of parameter value ($p < 0.01$, Figure 1B). In addition, this demonstrates that the spatially resolved FRAP analysis yields information on gradients in behavior over distances as small as ~65 nm, well below the theoretical resolution of the microscope (~220 nm for 510-nm wavelength light).

Kinetochores Are Clustered at Positions of Most Rapid GFP-Tubulin Exchange

In our computational simulations, the location of kinetochore clustering was predicted to be the site of the most rapid GFP-tubulin FRAP (Figure 3A, white box). To test this prediction in live cells, we quantified the average location of the kinetochores (labeled with Cse4-GFP) relative to the site of the most rapid GFP-tubulin turnover or FRAP. For reference, Spc29-CFP and RFP was used to mark the spindle poles for cells with Cse4-GFP–labeled kinetochores and GFP-tubulin–labeled microtubules, respectively. Representative experimental fluorescence images are shown in Figure 3B. The Cse4-GFP fluorescence intensity or rate of GFP-tubulin recovery was plotted as a function of relative spindle position, and the two data sets were quantitatively compared. As shown in Figure 3C (green arrow), the average kinetochore position on either side of the equator in the yeast metaphase spindle corresponded to the location of most rapid GFP-tubulin FRAP (Figure 3C, orange arrow). Thus, kMT plus-end dynamics were greatest at the approximate site of kinetochore clustering.

kMT Minus-Ends Are ~50 nm from Spc29-RFP at the Spindle Poles

The mean distance between the centroid of the Cse4-GFP–labeled kinetochore cluster and Spc29-CFP at the poles was 430 nm (Table 2). This would be an accurate measure of the mean length of kMTs if the kMT minus-ends were located at the site within the SPB where Spc29-CFP is located. To determine the distance from Spc29 to the kMT minus-ends, we quantitatively evaluated the distribution of GFP-tubulin fluorescence near the Spc29-RFP pole marker (kMT minus-end). By using two-color fluorescence imaging, we are not constrained by the diffraction limit of resolution with a single wavelength. As shown in Figure 4A, the microscope PSF spreads out the fluorescence via diffraction of light through the microscope lens. This blurring effect prevented detection of the offset distance between the Spc29-RFP spindle pole marker and GFP-tubulin at the kMT minus-ends by the naked eye. Although this separation distance was not readily apparent by eye, we reasoned that the relative amount of GFP-tubulin–associated fluorescence at the pole would be more intense if kMT minus-ends were in close proximity to the Spc29 SPB marker (Figure 4A, 1), and less intense if kMT minus-ends were further from the Spc29 SPB marker (Figure 4A, 2). Thus, the intensity of GFP-Tub1 fluorescence near to the SPB marker was predicted to vary according to the magnitude of the offset between GFP-tubulin at the kMT minus-ends and the Spc29-RFP SPB marker (Figure 4, A and B). By simulating experimental yeast spindles and then convolving these simulations with the experimentally measured microscope PSF (model-convolution), quantitative predictions can be made for the relative amount of GFP-tubulin associated fluorescence in the "bin" at the spindle pole, as well as the bins nearby, using different values of the MT minus-end/Spc29 SPB marker offset (Figure 4, B and C). Using this approach, we estimated the kMT minus-end position to be ~50 nm from the centroid of the Spc29-RFP fluorescence. Subtracting this distance from the

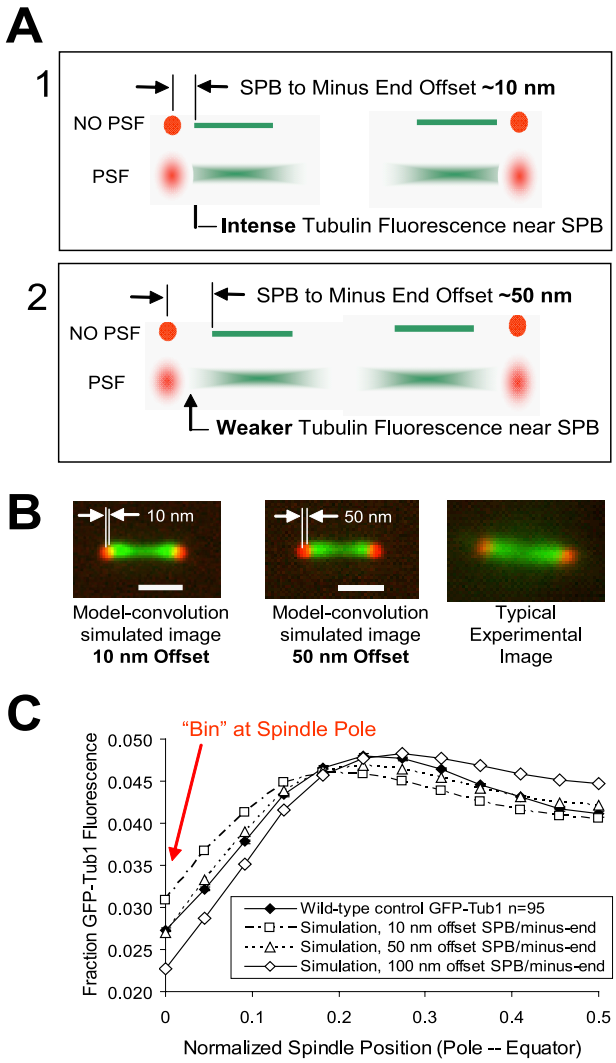

Figure 4. The microtubule minus ends are on average ~50 nm from the SPB. (A) Box 1, the upper spindle depicts an offset of ~10 nm between the SPB marker and the kMT minus-end in a theoretical image with no spreading of light through the microscope lens (point spread function [PSF]). In the box 1 lower image, the spreading of light due to PSF is depicted, resulting in a relatively intense GFP-Tub1 signal near the SPB marker. Box 2, the upper spindle depicts an offset of ~50 nm between the SPB marker and the kMT minus-end in a theoretical image with no spreading of light through the microscope lens (PSF). In the box 2 lower image, the spreading of light due to PSF is depicted, resulting in a relatively weak GFP-Tub1 signal near the SPB marker. (B) Images were simulated via model-convolution with 10 and 50 nm of offset between the SPB marker and kMT minus-ends (left two panels). A representative experimental image is displayed on the right. (C) Quantitative fluorescence analysis for mean GFP-tubulin fluorescence values by spindle position. Experimental and simulated curves represent average values over 92 spindles. All simulations assume that ipMT lengths are 89 ± 10% of spindle length and that the SPB marker is aligned at the edge of the starting bin during image analysis, such that offsets up to 65 nm are fully contained within bin "0." Red arrow denotes relative GFP-tubulin fluorescence in bin "0" near the SPB. By comparing experimentally measured GFP-tubulin at the poles to simulated image predictions the kMT minus-end position is estimated to be ~50 nm from the centroid of the Spc29-RFP fluorescence.

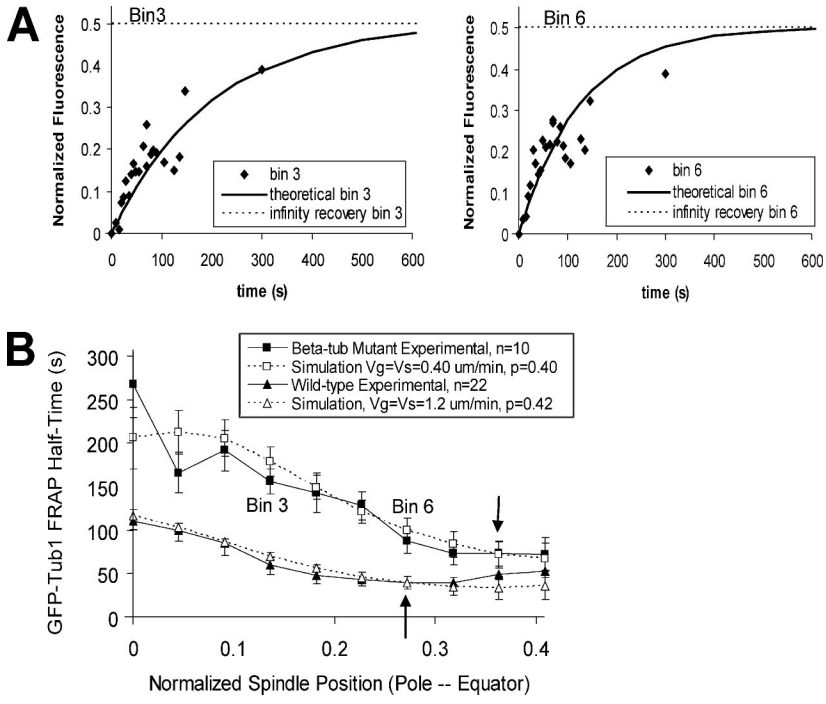

Figure 5. Reduced microtubule dynamicity alters the spatial gradient in tubulin turnover and kinetochore localization. (A) Representative raw GFP-Tub1 FRAP data for a β-tubulin (*tub2C254S*) mutant from a bin near the SPB (left) and another bin midway between the spindle equator and the SPB (right). Theoretical exponential fit curves calculated based on best-fit half-times by bin are drawn through each plot (solid line). (B) Experimental and simulated GFP-Tub1 FRAP for the β-tubulin mutant with reduced microtubule dynamicity compared with wild-type spindles. The rate of tubulin turnover was decreased in the β-tubulin mutant, especially near the SPB. The position of most rapid FRAP was shifted toward the spindle equator in the β-tubulin mutant (arrows). Simulation parameters and probability-of-fit (p values) for the fit of the experimental data to the simulation are listed in Table 1.

length between Cse4-GFP and Spc29-CFP gives a mean length for kinetochore microtubules at metaphase of ~380 nm, similar to that measured by EM studies (~390 nm; Winey *et al.*, 1995). Thus, the model-convolution method extracts spatial information below the resolution limit of the light microscope and enables an accurate measurement of average kMT lengths.

The Spatial Gradient in Tubulin Turnover Persists even When kMT Dynamicity Is Reduced by a β-Tubulin Mutant

We next asked how the experimentally observed spatial gradient in tubulin turnover rate would be affected by a mutation that resulted in reduced dynamics at kMT plus-ends. In this case, reduced microtubule dynamicity, or the number of tubulin subunits exchanged over time, may increase the time required for kinetochore alignment in prometaphase, but not necessarily affect kinetochore position or distribution. The parameters of dynamics have been measured for the plus-ends of cytoplasmic microtubules in the β-tubulin mutant (*tub2C354S*; Gupta *et al.*, 2002; Table 1). With this mutation, microtubule dynamicity is reduced throughout the cell cycle, resulting in reduced rates of spindle elongation and slower cellular growth. As was previously observed, GFP-tubulin FRAP rates were also significantly slowed in this mutant strain (Gupta *et al.*, 2002; Figure 5A; Table 2). Using high-resolution FRAP to analyze mutant spindle dynamics, a gradient in recovery half-times was observed (Figure 5B). This gradient is similar to wild-type spindles, but recoveries proceed on a slower time scale at both kinetochores and spindle poles. FRAP half-times near the SPBs were ~200 s, with the most rapid half-times ~90 s near the spindle equator (Figure 5, A and B). Thus, plus-end clustering during metaphase is likely maintained in the β-tubulin mutant spindles, despite reduced microtubule plus-end dynamics.

Computer Modeling Predicts Single Kinetochore Dynamics in the β-Tubulin Mutation

By reproducing the experimentally observed high-resolution FRAP results in both wild-type and β-tubulin mutant spindles, we can simulate the microtubule plus-end dynamics at single kinetochores in yeast (Table 1; Supplementary Movies 1 and 2). In these simulations, kMT growth and shortening rates are assumed to be constant and equal to each other over the length of the spindle. Simulation of the high-resolution FRAP experiment in the β-tubulin mutant spindles required a threefold decrease in kMT growth and shortening velocities (Supplementary Movie 2). Because of this decrease, simulated kMT plus-end excursion lengths were reduced, and there were significantly fewer instances of kMT plus-end depolymerization to the SPB (Figure 6, A and B; Supplementary Movies 1 and 2). As a result, the simulated distribution for plus-end visits to each spindle position was narrowed, indicating a reduction in amplitude of kinetochore oscillations (Figure 6C, red histogram represents a 31% reduction in kMT length SD). This was the result of reduced excursions away from the average cluster position (Figure 1A, arrows). The narrowed distribution of plus-end visits to each spindle position in the β-tubulin mutant simulation predicted that the gradient in tubulin turnover rates over the spindle length will be preserved in spindles with reduced microtubule dynamicity (Figure 5B).

The β-Tubulin Mutation Alters the Distribution of Kinetochore Clusters

The experimentally observed location of most rapid FRAP was shifted slightly toward the spindle equator in the β-tubulin mutant (Figure 5B; arrows depict shift in approximate location of fastest FRAP). This shift indicated that kMTs are longer, and thus kinetochore clusters in β-tubulin mutants would be predicted to be closer to the equator than in wild-type spindles. This result was confirmed experimentally by quantifying the centroid position of kinetochore-associated Cse4-GFP fluores-

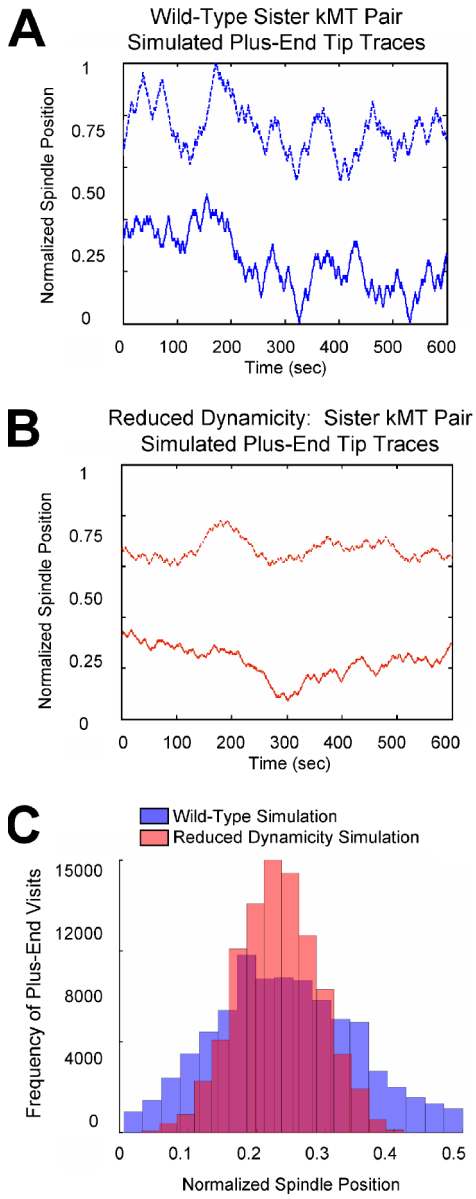

Figure 6. Simulation of kMT plus-end dynamics with reduced kMT growth and shortening velocity. (A) Spindle positions of a typical sister kinetochore pair over time in a wild-type simulation (Table 1). (B) Spindle positions of a typical sister kinetochore pair over time in a simulation with kMT growth and shortening velocities reduced threefold (Table 1). Kinetochores in the simulation with reduced kMT velocities made shorter excursions as compared with wild-type controls. (C) Simulated frequency of plus-end positions by spindle location; frequency of simulated wild-type plus-end position by spindle location, blue; frequency of plus-end position by spindle location in simulation with reduced kMT growth and shortening velocities, red; overlap zone between wild-type and slow velocity histograms, purple. In simulations with reduced growth and shortening velocities, the distribution of plus-end positions by spindle location is narrowed (36% reduction in the SD of kMT length).

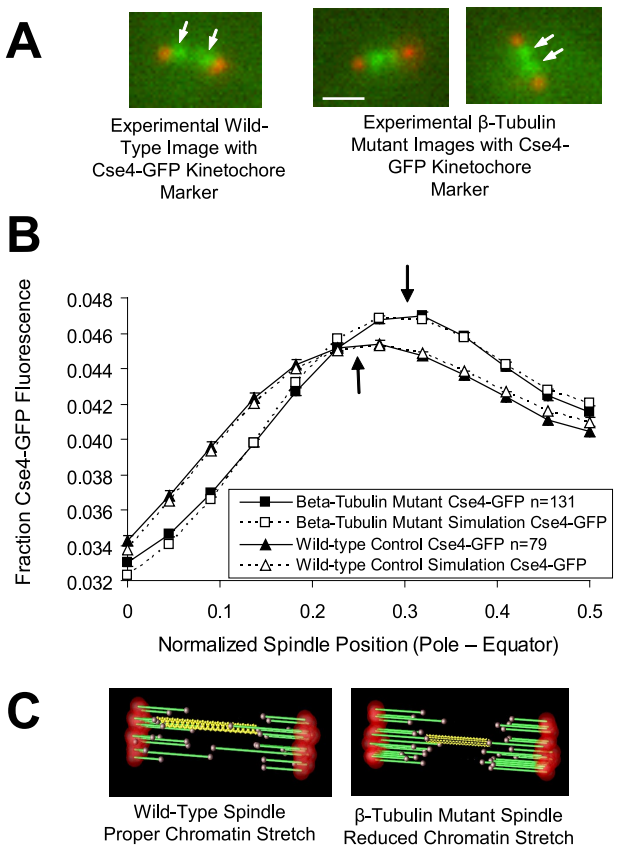

Figure 7. A β-tubulin mutation with reduced microtubule dynamicity has tightly clustered kinetochores and reduced kinetochore tension (A) Wild-type and β-tubulin mutant spindles (Cse4-GFP, green; Spc29-CFP, red). Scale bar, 1000 nm. White arrows denote kinetochore clusters, which is shifted toward the spindle equator in the β-tubulin mutant. (B) Experimental and simulated comparison of kinetochore fluorescence (Cse4-GFP) in the β-tubulin mutant compared with wild-type. The peak kinetochore position is shifted toward the spindle equator in the β-tubulin mutant, such that sister kinetochore spacing is reduced. In addition, the kinetochore-associated fluorescence distribution curve reveals a sharp peak in Cse4-GFP fluorescence in the β-tubulin mutant, indicating that kinetochores are more tightly clustered within a half-spindle in the β-tubulin mutants compared with wild-type spindles. (C) Representative simulated animations of wild-type and β-tubulin mutants (Supplementary Movies 1 and 2). In the simulation, a slight bias toward plus-end assembly of the β-tubulin mutant resulted in longer kMTs and reduced chromatin stretch (chromatin "spring" shown in yellow).

cence relative to Spc29-CFP pole fluorescence in the β-tubulin mutant (Figure 7A, white arrows). The distance between kinetochore clusters was decreased by ~25% in the β-tubulin mutant, whereas the average spindle length changed little (Figure 7, B and C; Table 2). After correcting for the distance between Spc29-CFP and the kMT minus-ends (see above), the mean predicted kMT length was ~440 nm in the β-tubulin mutant, ~60 nm longer on average than wild-type kMTs.

As predicted by simulations with reduced kMT growth and shortening velocities, the experimentally observed distribution of kinetochore-associated fluorescence within each sister cluster was also narrowed in the β-tubulin mutant (31% reduction in the SD of the experimental kMT lengths measured via variance in Cse4-GFP fluorescence; Table 2; Figure 7B). By quantifying Cse4-GFP fluorescence in the β-tubulin mutant, kinetochore clustering was found to be 31% more tightly focused on either side of the spindle equator than with wild-type spindles.

Reduced Tension between Sister Kinetochores Correlates with Centromere Plasmid Mis-Segregation

To test if reduced kMT dynamics and tension had an effect on the fidelity of chromosome segregation, we performed

centromere-plasmid loss experiments in the β-tubulin mutant. Centromere plasmids were lost at a 2.5-fold greater frequency in *tub2C354S* containing cells (wild-type, 4.9 ± 0.4% loss/generation; β-tubulin mutant, 12.0 ± 0.4% loss/generation). This suggests that there may be tension-dependent chromosome mis-segregation as a result of altered kMT dynamics.

DISCUSSION

Using computer modeling and high-resolution FRAP, we predicted theoretically and observed experimentally the existence of a spatial gradient in kMT turnover in metaphase budding yeast cells. The methodology enabled detection of a gradient in GFP-tubulin FRAP over distances as small as ~65 nm. We found that the most rapid GFP-tubulin turnover occurred where the kMT plus-ends and kinetochores were located. A β-tubulin mutant with reduced microtubule dynamicity also exhibited a gradient in GFP-tubulin turnover and a tighter clustering of kinetochores. The tubulin mutant had slightly longer kMTs and less tension between sister kinetochores, as well as increased chromosome loss.

High-Resolution FRAP Analysis

Through the use of digital light microscopy experiments designed in concert with computational simulations, we have developed a spatially resolved GFP-tubulin FRAP assay that simultaneously characterizes both the clustering of kMT plus-end locations and the dynamics of kMTs in the yeast metaphase spindle (Figure 2). kMT plus-end turnover is greatest at the site of kinetochore clustering in the yeast metaphase spindle, and GFP-tubulin FRAP proceeds in a "wave" toward each SPB. FRAP half-times at the SPB are nearly threefold slower than FRAP half-times midway between the spindle equator and each SPB (the site of kinetochore positioning), indicating that kMT plus-ends infrequently depolymerize to the poles. Because half-times separated by one pixel, corresponding to ~65 nm, were in some cases statistically different ($p < 0.01$ by t test, Supplementary Table S1), the FRAP analysis can resolve differences in microtubule dynamics at distances less than the theoretical resolution of the microscope (~220 nm for 510-nm light). Thus, the light microscope has the ability to gain spatially resolved information on protein dynamics in vivo at nanometer-scale distances, limited only by the size of the data set and the distance projected onto single detector elements of the digital camera detector array.

Using two-color digital imaging with model convolution techniques, we quantified the average distance between the centroid of Spc29-RFP– or CFP-labeled SPBs and kMT minus-ends (~50 nm). Using this offset, we then estimated the average kMT length based on the separation between kinetochore clusters (Cse4-GFP) and kMT minus-ends (~380 nm in WT spindles). This length also corresponds well with kMTs length as measured by electron microscopy (~390 nm; Winey *et al.*, 1995). The combination of approaches has now enabled high-resolution length measurements of metaphase spindles using the light microscope.

High-Resolution FRAP Constrains Simulation Models of kMT Dynamic Instability

Our observation that kinetochore clustering corresponds to the location of most rapid FRAP in the yeast metaphase spindle indicates that kMT plus-ends are dynamic and that kinetochores remain in close proximity to dynamic kMT plus-ends. Clustering of dynamic plus-ends on either side of the spindle equator with relatively infrequent excursions to the SPBs argues for precise regulation of kMT plus-end dynamics. The simulation, which relies on high catastrophe frequency at the spindle equator with rescue frequency promoted by tension generated via chromatin stretch between sister kinetochores, reproduces the kMT dynamics as were observed in the high-resolution FRAP experiments (Figure 5B). The GFP-tubulin FRAP simulation constrains kMT growth and shortening rates to a narrow range of values (Table 1) and also rules out simpler models, such as simple stochastic dynamic instability (Figure 1B), for the regulation of kMT dynamic instability in both wild-type and β-tubulin mutant yeast spindles. Both the wild-type and β-tubulin mutant simulation parameter values are similar to the growth and shortening rates that were experimentally observed for cytoplasmic microtubules (Table 1; Gupta *et al.*, 2002). However, the estimated catastrophe and rescue frequencies are much higher for kMTs than for cytoplasmic MTs, indicating that the kinetochore regulates growth and shortening excursions within the spindle. Changes in plus-end dynamics have also been observed for kinetochore attached MTs compared with cytoplasmic microtubules in G1 cells (Dorn *et al.*, 2005). In addition, the catastrophe and rescue frequencies used to model the wild-type and β-tubulin mutant were nearly identical, indicating that the oscillations associated with dynamic instability are dictated by the kinetochore and are robust with respect to perturbation of tubulin itself.

Estimation of an Upper Limit to Poleward kMT Flux

Recently, experimental and modeling studies have highlighted the importance of poleward microtubule flux in creating tension at the kinetochores (Maddox *et al.*, 2003; Civelekoglu-Scholey *et al.*, 2006). It was proposed that chromosome oscillations occur in systems with little or no flux, such as in yeast, to compensate for the lack of poleward flux to generate tension at the kinetochore (Maddox *et al.*, 2000; Tanaka *et al.*, 2005). Although poleward kMT flux has not been detected previously in budding yeast (Maddox *et al.*, 2000; Tanaka *et al.*, 2005), it may be that the spatial resolution was insufficient to detect flux in an intact wild-type spindle.

By calculating a FRAP half-time specifically at the SPB, our analysis places a theoretical upper limit on the rate of poleward kMT flux in yeast metaphase spindles. If the spindle depended only on poleward flux for recovery, then the fastest flux rate that would be consistent with the GFP-tubulin FRAP data are ~0.10 μm/min. We estimated this upper limit as follows: assuming total 220 s to achieve recovery at poles (twice the experimentally observed half-time) and an average kMT length of ~380 nm: (~380-nm mean kMT length)/(220 s to recovery) = 1.7 nm/s = 0.10 μm/min rate of poleward flux. The flux rate would be even slower with a combination of kMT plus-end dynamics and poleward flux. The theoretical maximum rate (0.1 μm/min) is significantly slower than the rate of polymerization and depolymerization at kinetochores based on measurements of centromere movements using lacO-GFP markers placed ~1 kb from the centromere (1.5 μm/min; Pearson *et al.*, 2001) and based on the growth and shortening rates used here to match the observed tubulin FRAP recovery rates (Table 1). Therefore, the theoretical flux limit calculated here would not significantly contribute to the observed chromosome motility.

A Bias toward kMT Assembly Results in Loss of Tension at the Kinetochore

The decrease in GFP-tubulin turnover rate near the SPB in the β-tubulin mutant suggests that kMT plus-end excursion lengths are significantly reduced in frequency compared with wild-type spindles (Figure 6), with a shift of kMT plus-ends toward the spindle equator (Figure 7). Although we do not understand the mechanism for this shift, these observations suggest that reduced kinetochore tension in the β-tubulin mutant results specifically from a net increase in kMT plus-end polymerization (Figure 7C). This result is consistent with cells treated with taxol or low concentrations of nocodazole where MT dynamics and centromere tension are also decreased (Vasquez *et al.*, 1997; Waters *et al.*, 1998). Thus, force-generating kMT plus-end dynamics are critical to establish separation between sisters and to maintain tension at the kinetochore.

Loss in Kinetochore Tension and the Fidelity of Chromosome Segregation

The β-tubulin mutation resulted in tighter kinetochore clustering and a moderate loss of tension at the kinetochore (~25% loss in tension; Figure 7, A–C). The observed increase in centromere plasmid loss in the mutant suggests that even a subtle loss in tension at the kinetochore has consequences for the fidelity of chromosome segregation. We hypothesize that a persistent loss in tension at the kinetochore may result in transient kinetochore-kMT detachment via a tension-dependent mechanism (Nicklas, 1997; Pinsky and Biggins, 2005). At least two alternative possibilities exist for how chromosome loss occurs in the β-tubulin mutant. First, it may be that kMT plus-end dynamics and, therefore, excursions are required for error correction. Tight clustering of kinetochores indicates that kMT plus-ends are more constrained than in normal conditions (~31% reduction in the SD of the kMT length). Robust kMT plus-end dynamics may allow for mechanical detachment of improper attachments and subsequent error correction. Second, it is possible that reduced MT dynamicity could affect "search and capture" for unattached kinetochores, resulting in a decreased number of attached kinetochores. We do not believe that erroneous search and capture is the dominant cause for chromosome loss because kinetochores are tightly clustered in the location of most rapid FRAP in the β-tubulin mutant, suggesting that MT plus-ends are localized with and attached to kinetochores.

In conclusion, we have combined simulation and experimental methodologies to improve the resolution of GFP-tubulin FRAP to detect a spatial gradient in kMT turnover at distances of ~65 nm. Analysis of fluorescence recovery patterns enabled high-resolution tracking of kinetochore and kMT plus-end positions in the yeast metaphase spindle. Although kMT plus-ends remain highly dynamic during yeast metaphase, these dynamics are tightly regulated to allow for proper kinetochore positioning and separation. We find that regulated kMT plus-end dynamics are necessary for normal sister separation and accurate chromosome segregation by defining the position of kinetochores on the spindle axis. Spatially resolved FRAP on the nanometer-scale will be a valuable tool for future studies aimed at characterizing fluorescent protein dynamics and localization in this genetically tractable organism (Shimagawa *et al.*, 2006). In addition, it will aid studies of submicrometer-sized structures within larger cells.

ACKNOWLEDGMENTS

We thank Drs. Dick Himes and Moe Gupta for generous contribution of the β-tubulin strains. We thank Julian Haase for help with strain construction. Thanks to Drs. Paul Maddox, Jennifer Deluca, and Jason Stumpff for critical comments on the manuscript and discussions. This work was supported by National Institutes of Health (NIH) Grants GM32238 (K.B.), GM071522 (D.J.O.), and GM24364 (E.D.S.). C.G.P. is supported by a Damon Runyan Fellowship. M.K.G. is supported by an NIH predoctoral fellowship. L.V.P. is supported by a SPIRE fellowship (GM00678).

REFERENCES

Bullitt, E., Rout, M. P., Kilmartin, J. V., and Akey, C. W. (1997). The yeast spindle pole body is assembled around a central crystal of Spc42p. Cell *89*, 1077–1086.

Byers, B., Shriver, K., and Goetsch, L. (1978). The role of spindle pole bodies and modified microtubule ends in the initiation of microtubule assembly in *Saccharomyces cerevisiae*. J. Cell Sci. *30*, 331–352.

Chen, Y., Baker, R. E., Keith, K. C., Harris, K., Stoler, S., and Fitzgerald-Hayes, M. (2000). The N terminus of the centromere H3-like protein Cse4p performs an essential function distinct from that of the histone fold domain. Mol. Cell. Biol. *20*, 7037–7048.

Civelekoglu-Scholey, G., Sharp, D. J., Mogilner, A., and Scholey, J. M. (2006). Model of chromosome motility in *Drosophila* embryos: adaptation of a general mechanism for rapid mitosis. Biophys. J. *13*, 3966–3982.

Dorn, J. F., Jaqaman, K., Rines, D. R., Jelson, G. S., Sorger, P. K., and Danuser, G. (2005). Yeast kinetochore microtubule dynamics analyzed by high-resolution three-dimensional microscopy. Biophys. J. *89*, 2835–2854.

Fowles, G. R. (1975). Introduction to Modern Optics, 2nd Ed., New York: Dover, 117–120.

Gardner, M. K., Pearson, C. G., Sprague, B. L., Zarzar, T. R., Bloom, K., Salmon, E. D., and Odde, D. J. (2005). Tension-dependent regulation of microtubule dynamics at kinetochores can explain metaphase congression in yeast. Mol. Biol. Cell *16*, 3764–3775.

Goshima, G., and Yanagida, M. (2000). Establishing biorientation occurs with precocious separation of the sister kinetochores, but not the arms, in the early spindle of budding yeast. Cell *100*, 619–633.

Gupta, M. L., Jr., Bode, C. J., Thrower, D. A., Pearson, C. G., Suprenant, K. A., Bloom, K. S., and Himes, R. H. (2002). beta-tubulin C354 mutations that severely decrease microtubule dynamics do not prevent nuclear migration in yeast. Mol. Biol. Cell *13*, 2919–2932.

He, X., Asthana, S., and Sorger, P. K. (2000). Transient sister chromatid separation and elastic deformation of chromosomes during mitosis in budding yeast. Cell *101*, 763–775.

Inoue, S., and Salmon, E. D. (1995). Force generation by microtubule assembly/disassembly in mitosis and related movements. Mol. Biol. Cell *6*, 1619–1640.

Kapoor, T. M., and Compton, D. A. (2002). Searching for the middle ground: mechanisms of chromosome alignment during mitosis. J. Cell Biol. *157*, 551–556.

Maddox, P., Bloom, K., and Salmon, E. D. (2000). Polarity and dynamics of microtubule assembly in the budding yeast *Saccharomyces cerevisiae*. Nat. Cell Biol. *2*, 36–41.

Maddox, P., Straight, A., Coughlin, P., Mitchison, T. J., and Salmon, E. D. (2003). Direct observation of microtubule dynamics at kinetochores in *Xenopus* extract spindles: implications for spindle mechanics. J. Cell Biol. *162*, 377–382.

Mitchison, T. J. (2005). Mechanism and function of poleward flux in *Xenopus* extract meiotic spindles. Philos. Trans. R. Soc. Lond. B. Biol. Sci. *360*, 623–629.

Nicklas, R. B. (1997). How cells get the right chromosomes. Science *275*, 632–637.

O'Toole, E. T., Winey, M., and McIntosh, J. R. (1999). High-voltage electron tomography of spindle pole bodies and early mitotic spindles in the yeast *Saccharomyces cerevisiae*. Mol. Biol. Cell *10*, 2017–2031.

Pearson, C. G., Maddox, P. S., Salmon, E. D., and Bloom, K. (2001). Budding yeast chromosome structure and dynamics during mitosis. J. Cell Biol. *152*, 1255–1266.

Pearson, C. G., Maddox, P. S., Zarzar, T. R., Salmon, E. D., and Bloom, K. (2003). Yeast kinetochores do not stabilize Stu2p-dependent spindle microtubule dynamics. Mol. Biol. Cell *14*, 4181–4195.

Pearson, C. G., Yeh, E., Gardner, M., Odde, D., Salmon, E. D., and Bloom, K. (2004). Stable kinetochore-microtubule attachment constrains centromere positioning in metaphase. Curr. Biol. *14*, 1962–1967.

Peterson, J. B., and Ris, H. (1976). Electron-microscopic study of the spindle and chromosome movement in the yeast *Saccharomyces cerevisiae*. J. Cell Sci. *22*, 219–242.

Pinsky, B. A., and Biggins, S. (2005). The spindle checkpoint: tension versus attachment. Trends Cell Biol. *15*, 486–493.

Rout, M. P., and Kilmartin, J. V. (1990). Components of the yeast spindle and spindle pole body. J. Cell Biol. *111*, 1913–1927.

Shimagawa, M. M., *et al*. (2006). Mps1 phosphorylation of the kinetochore component Dam1 couples kinetochores to microtubule plus-ends at metaphase. Curr. Biol. (*in press*).

Sprague, B. L., Pearson, C. G., Maddox, P. S., Bloom, K. S., Salmon, E. D., and Odde, D. J. (2003). Mechanisms of microtubule-based kinetochore positioning in the yeast metaphase spindle. Biophys. J. *84*, 3529–3546.

Tanaka, K., Mukae, N., Dewar, H., van Breugel, M., James, E. K., Prescott, A. R., Antony, C., and Tanaka, T. U. (2005). Molecular mechanisms of kinetochore capture by spindle microtubules. Nature *434*, 987–994.

Tanaka, T., Fuchs, J., Loidl, J., and Nasmyth, K. (2000). Cohesin ensures bipolar attachment of microtubules to sister centromeres and resists their precocious separation. Nat. Cell Biol. *2*, 492–499.

Vasquez, R. J., Howell, B., Yvon, A. M., Wadsworth, P., and Cassimeris, L. (1997). Nanomolar concentrations of nocodazole alter microtubule dynamic instability in vivo and in vitro. Mol. Biol. Cell *8*, 973–985.

Waters, J. C., Chen, R. H., Murray, A. W., and Salmon, E. D. (1998). Localization of Mad2 to kinetochores depends on microtubule attachment, not tension. J. Cell Biol. *141*, 1181–1191.

Winey, M., Mamay, C. L., O' Toole, E. T., Mastronarde, D. N., Giddings, T. H., Jr., McDonald, K. L., and McIntosh, J. R. (1995). Three-dimensional ultrastructural analysis of the *Saccharomyces cerevisiae* mitotic spindle. J. Cell Biol. *129*, 1601–1615.